CHALMERS
UNIVERSITY OF TECHNOLOGY

Optical Characterization of Marine Aerosols Using a Morphologically Realistic Model With Varying Water Content: Implications for Lidar

Geophysical Research Letters

RESEARCH LETTER
10.1029/2023GL107541

Key Points:

- Modeled extinction coefficient of marine aerosol depends on particle radius and wavelength, but not on water content
- The depolarization ratio and the color ratio of the backscattering cross section generally decrease with growing aerosol water content
- The linear polarization peak near backscattering angles at NIR wavelength could be used in passive polarimetry to retrieve water content

Correspondence to:
M. Kahnert,
michael.kahnert@smhi.se

Citation:
Kahnert, M., & Kanngießer, F. (2024). Optical characterization of marine aerosols using a morphologically realistic model with varying water content: Implications for lidar applications and passive polarimetric remote sensing. *Geophysical Research Letters*, *51*, e2023GL107541. https://doi.org/10.1029/2023GL107541

Received 27 NOV 2023
Accepted 13 FEB 2024

Author Contributions:
Conceptualization: M. Kahnert, F. Kanngießer
Data curation: M. Kahnert, F. Kanngießer
Formal analysis: M. Kahnert
Funding acquisition: M. Kahnert
Methodology: M. Kahnert, F. Kanngießer
Project administration: M. Kahnert
Writing – original draft: M. Kahnert
Writing – review & editing: F. Kanngießer

Optical Characterization of Marine Aerosols Using a Morphologically Realistic Model With Varying Water Content: Implications for Lidar Applications and Passive Polarimetric Remote Sensing

M. Kahnert[1,2] **and F. Kanngießer**[3]

[1]Research Department, Swedish Meteorological and Hydrological Institute, Norrköping, Sweden, [2]Department of Space, Earth and Environment, Chalmers University of Technology, Gothenburg, Sweden, [3]GEOMAR Helmholtz Center for Ocean Research Kiel, Wischhofstr, Germany

Abstract Retrieving the physical properties and water content of marine aerosols requires understanding the links between the particles' optical and microphysical properties. By using a morphologically realistic model with varying salt mass fractions f_m, describing the transition from irregularly shaped, dry salt crystals to brine-coated geometries, optical properties relevant to polarimetric remote sensing are computed at wavelengths of 532 and 1,064 nm. The extinction cross section and its color ratio depend on particle size, but are insensitive to changes in f_m; thus, measured extinction coefficients at two wavelengths contain information on both particle number and size. The lidar ratio's dependence on both size and wavelength has implications for inverting the lidar equation. The results suggest that active observations of the backscattering cross section's color ratio and the depolarization ratio, as well as, passive observations of the degree of linear polarization offer avenues to obtain the water content of marine aerosols.

Plain Language Summary Salt aerosols ejected into air from the ocean surface are the most abundant type of particles in the atmosphere. Clouds form by condensation onto these particles, which, in turn, reflect, absorb, and emit light and thermal radiation, thereby influencing the climate system. To better describe these processes in models, one needs to monitor salt aerosols from satellites. The main difficulty is to obtain information on the particles' concentration, size, and water content from satellite measurements that can only observe light scattered by the aerosols. In this study a model is being employed to study how the shape, size, and composition of marine aerosols impact their light-scattering properties. The results suggest that the extinction of light measured at two wavelengths provides a robust method for obtaining the concentration and size of the particles. The water content can be obtained from observing the intensity of backscattered laser light at two wavelengths, or the change in polarization of the backscattered light at a single wavelength. One can also observe the polarization of scattered near-infrared sunlight close to the backscattering direction to obtain information on the water content of the particles.

1. Introduction

Global sea salt emissions amount to more than 4,700 Tg/year, which exceeds emissions of all other types of aerosols combined (H. Wang et al., 2020). Sea salt acts as cloud condensation nuclei, thus influencing cloud optical properties, cloud lifetime, and the hydrological cycle. This amounts to a substantial effect on the radiative balance in the climate system, owing to the high amount of global emissions, the vast extent of marine cloud fields, and the high albedo contrast between clouds and the ocean surface. Also, long-range transported marine aerosols are important for ecosystem modeling, because deposition of sea salt over land can counteract the effect of acidifying pollutants.

In aerosol transport models, one simulates emission of marine aerosols from bubble bursting and spume drops by use of empirical parameterizations (Soares et al., 2016; Sofiev et al., 2011) that are derived from laboratory observations (Mårtensson et al., 2003; Monahan et al., 1986). The number density of emitted particles depends on the surface wind speed, while the size distribution is dependent on sea-surface temperature and salinity (Sofiev et al., 2011). Hygroscopic growth of marine particles is important to accurately describe gravitational settling and dry deposition, as well as optical properties (Soares et al., 2016). The wet radius of the particles can be computed

from their dry radius and the ambient relative humidity by use of Köhler theory (Z. Wang et al., 2019) or by approximate formulas (Fitzgerald, 1975). However, solving these equations can be time-consuming. Therefore, in large-scale aerosol transport models one typically employs simple empirical parameterizations of the wet radius as a function of dry radius and relative humidity (Gerber, 1985; Sofiev et al., 2011).

How can we evaluate parameterizations of marine aerosol emission fluxes, size distribution, and hygroscopic growth on the regional and global scale? Satellite observations provide consistent long-term data records with global coverage that can, potentially, be used to constrain models and to improve parameterizations of aerosol emission and water content. A recent analysis of a 10-year data record of CALIPSO observations during winter months over the Southern Ocean (Thomas et al., 2022) revealed that the backscattering coefficient increases with surface wind speed, while the depolarization ratio monotonically decreases with growing relative humidity. This can be understood in terms of an increase in the emission flux with wind speed, and an increase in water content with increasing relative humidity (which makes the particles more spherical, thus less depolarizing). A similar relation between depolarization and relative humidity in marine aerosols has been reported from lidar campaign measurements (Haarig et al., 2017) and from airborne campaigns (Ferrare et al., 2023).

This illustrates the potential usefulness of satellite data in studying emission and water adsorption processes of marine aerosols. However, these studies presently only provide a qualitative interpretation of physical aerosol properties in terms of observed optical properties. Further progress will depend on a better understanding of the relation between physical and optical properties. A most challenging problem is to understand how complex morphological properties, such as irregularly shaped salt crystals and the inhomogeneous composition of partially dissolved, water-coated crystals, manifest themselves in polarimetric optical properties, which are known to be highly sensitive to morphology and composition. Here, a morphologically realistic model for marine aerosols is employed to investigate which optical parameters are most promising for obtaining information on particle number density, effective radius, and water content. This study is of high relevance for the interpretation of observations by the Aerosol and Carbon dioxide Detection Lidar onboard the DQ-1 satellite, a High Spectral Resolution Lidar with polarization detection capabilities, which uses wavelengths of 532 and 1,064 nm (Dai et al., 2023; Liu et al., 2023). Also, accounting for the impact of inhomogeneity in brine-coated salt aerosols on optical properties can be important for modeling the direct radiative forcing effect of marine aerosols (Z. Wang et al., 2019) and the radiative impact on precipitation in tropical cyclones (Zhu et al., 2022).

It is noted that there have been a number of different model particles in use for marine aerosols, such as cubes (David et al., 2013), distorted cubes (Kanngießer & Kahnert, 2021a), homogeneous superellipsoids (Bi, Lin, Liu, & Zhang, 2018; Kanngießer & Kahnert, 2021b), inhomogeneous superspheroids (Bi, Lin, Wang, et al., 2018; Kanngießer & Kahnert, 2021b), cube-sphere hybrid particles (Kanngießer & Kahnert, 2021b), and non-concentric core-mantle spheres (Kanngießer & Kahnert, 2021b). All of these particles introduce various simplifying assumptions, the validity of which are not yet fully explored. However, a recent comparison of our reference model with homogeneous superellipsoids (Kanngießer & Kahnert, 2021b) revealed that by a suitable tuning of the roundness parameter and aspect ratio of the superellipsoids one can reasonably well reproduce the lidar ratio and backscatter linear depolarization ratio obtained with the reference model at 532 nm. Also, the results in Bi, Lin, Wang, et al. (2018) show that variation of the roundness parameter and aspect ratio of super-spheroids results in a significant variation in the linear depolarization ratio, which indicates that this model is highly tunable. A main advantage of simplified models is that they allow for simplifications in numerical computations, while a main concern is their robustness. An instance of a simple model that has been tuned to reproduce specific optical properties at a certain wavelength may not be applicable to other optical properties or wavelengths.

2. Methods

2.1. Particle Model

While pure sodium chloride crystals display cubic shape, dry marine aerosols in nature are often irregular particles resembling distorted cubes (Gwaze et al., 2007; Haarig et al., 2017; King et al., 2012; McInnes et al., 1994; Patterson et al., 2016; Peart & Evans, 2011; Wise et al., 2005; Zeng et al., 2013). Polarimetric optical properties of marine particles are well described by a realistic distorted cube model based on convex polyhedra, which was developed in Kanngießer and Kahnert (2021a). Figure 1 (top row) shows four stochastic realizations of that model.

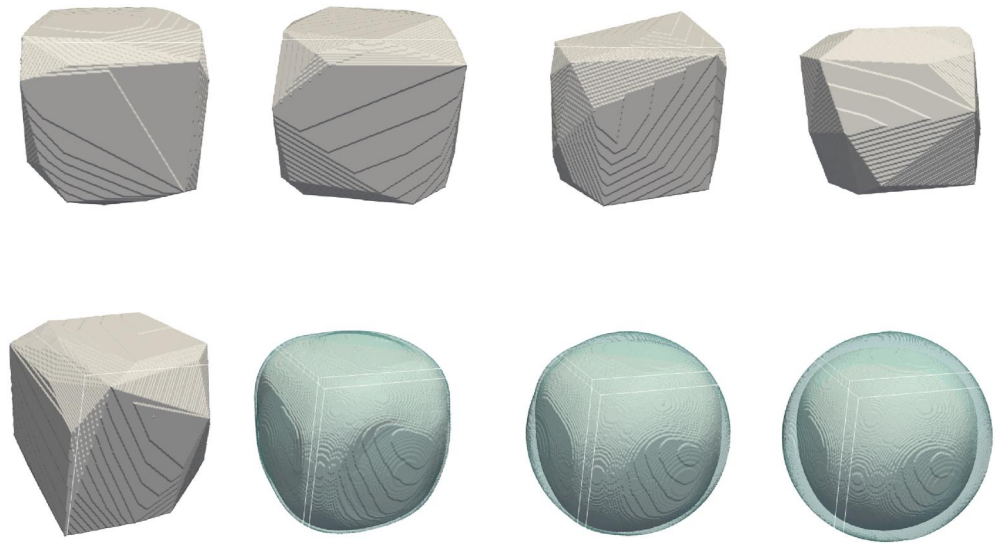

Figure 1. Top: four stochastic realizations of the convex polyhedra model for dry marine aerosols; bottom: model particles with decreasing salt mass fractions (from left to right) f_m = 1.00, 0.97, 0.94, and 0.91.

Condensation of water modulates the optical properties. Here, the model described in Kahnert and Kanngießer (2023a) is employed, which uses a pseudo-potential model (Ishimoto et al., 2019) to realistically describe the morphological changes due to condensation of water. More specifically, (a) water condenses first onto parts of the particle with a low surface potential (corresponding to a large number of neighboring atoms); (b) solid material in contact with the liquid coating is first dissolved at those points where the surface potential is high (corresponding to few neighboring atoms); (c) salt that becomes dissolved can be relocated so that the liquid coating becomes rearranged in a state of low surface potential; and (d) the brine coating consists of 36 g salt per 100 ml water with a density of 1,210 kg/m^3, while pure water and dry sea salt are assumed to have densities of 1,000 and 2,240 kg/m^3, respectively. Note that a mass-weighted average of the densities of salt and water would result in a density of 1,328 kg/m^3, which would be larger than the true density of brine. Thus, owing to the lower density of 1,210 kg/m^3, the composite particle of brine and salt has a larger volume than the sum of the volumes of salt and water. The model accounts for this effect in calculating the wet radius as a function of the dry radius and the salt-mass fraction. A detailed model description and the transformation from salt-volume fraction to salt-mass fractions is given in Kahnert and Kanngießer (2023a). Tests at a wavelength of 532 nm showed that the range of lidar ratios and linear depolarization ratios obtained with the model is consistent with existing field and satellite observations (Kahnert & Kanngießer, 2023a). Figure 1 (bottom row) shows four realization of the model with salt-mass fractions (from left to right) f_m = 1.00, 0.97, 0.94, 0.91, where $f_m = m_{salt}/(m_{salt} + m_{water})$, and m_{salt} and m_{water} represent the masses of salt and water in the composite particle.

The model is employed to generate 74 dry salt crystals with radii r = 0.04, 0.06, …, 1.5 μm, where r is the radius of a mass-equivalent sphere. (An upper cut-off of 1.5 μm had to be imposed due to numerical limitations in the light-scattering computations.) Each of these particles is a different stochastic realization of the distorted cube model (Kanngießer & Kahnert, 2021a), so that the ensemble of marine aerosols is described by a size-shape distribution. In addition to dry particles (f_m = 1.00), brine-coated model particles are generated for salt-mass fractions f_m = 0.97, 0.94, 0.91. As discussed in Kahnert and Kanngießer (2023a), and as illustrated in Figure 1 (bottom), this braces the range within which the transition from dry nonspherical to wet spherical marine particles occurs. Although it is not straightforward to relate these mass fractions to relative humidity, it is estimated that, for pure sodium chloride crystals, this range would roughly correspond to a relative humidity of 43%–48% for efflorescence, and 60%–72% for deliquescence (Kahnert & Kanngießer, 2023a). However, field and satellite observations of lidar depolarization ratios of marine aerosols as a function of relative humidity suggest that in nature the transition from dry depolarizing to wet non-depolarizing particles is rather smooth and extends over a broad range of the relative humidity between 40% and 90% (Haarig et al., 2017; Thomas et al., 2022).

2.2. Dielectric Properties and Light-Scattering Computations

The marine-aerosol model had previously been tested by modeling lidar-relevant quantities at a single wavelength of 532 nm (Kahnert & Kanngießer, 2023a; Kanngießer & Kahnert, 2021b). Here, a more comprehensive study is presented with additional computations at a wavelength of 1,064 nm (thus allowing the computation of color ratios), as well as an investigation of the degree of linear polarization and its dependence on wavelength. The degree of linear polarization is relevant for passive polarimetric remote sensing. Also, the optical properties at 532 nm have been computed here with an updated value of the complex refractive index of the brine coating, as explained below. As the light-scattering computations are numerically demanding, these computations required several months of wall-clock time.

At a wavelength of $\lambda = 532$ nm, the complex refractive indices of sea salt and brine are assumed to be $m = 1.5484 + 0\mathrm{i}$ (Eldridge & Palik, 1997) and $1.3844 + 2.5330 \cdot 10^{-8}\mathrm{i}$, respectively. The latter is an updated value different from the one in Kahnert and Kanngießer (2023a), which accounts for the corrigendum in X. Li et al. (2018) to the parameterization given in X. Li et al. (2015). At $\lambda = 1{,}064$ nm, the corresponding complex refractive indices are $1.5312 + 0\mathrm{i}$ and $1.3674 + 3.309 \cdot 10^{-5}\mathrm{i}$, respectively.

Optical properties were computed by use of the discrete-dipole approximation (DDA), using ADDA version 1.3b4 (Yurkin & Hoekstra, 2011). The particles were represented by a Cartesian grid of dipoles. The main parameter controlling the numerical accuracy of the solution is the number of dipoles per wavelength *dpl*. The optical properties were averaged over three Euler angles α, β, γ by use of Romberg integration, assuming randomly oriented particles. In ADDA, each Euler angle uses a range of subdivisions $J_{\min}$, $J_{\max}$. In this study, $dpl \geq 25$ is used, as well as $J_{\min} = 2$ and $J_{\max} = 4$ for α and γ in the interval [0, 360°], and $J_{\min} = 2$ and $J_{\max} = 3$ for β in the interval [0, 180°]. At these settings, the results of the computations have converged for this kind of particle geometry (Kanngießer & Kahnert, 2021a).

2.3. Size Distribution

The size distribution of marine aerosols is often modeled by either multi-modal lognormal or by power-law functions. What all models have in common is that the size distribution is rather broad. Here, the modified power-law distribution proposed by Sofiev et al. (2011) is used, given by

$$n(r) = N_1 \frac{\exp\left(\frac{-0.09}{2r+0.003}\right)}{2+\exp\left(\frac{-5}{2r}\right)} \cdot \frac{1+0.05(2r)^{1.05}}{(2r)^3} \cdot 10^{1.05\exp\left[-\left(\frac{0.27-\log(2r)}{1.1}\right)^2\right]} \cdot (2r)^{-\alpha}. \quad (1)$$

N_1 is proportional to the total number density, and the volume-equivalent dry radius r is given in μm. This model has been derived from two earlier models, which were based on observations of bubble-bursting aerosols and spume drops (Monahan et al., 1986) as well as laboratory measurements in a bubble chamber (Mårtensson et al., 2003). The model is used in several chemical transport models and parametrizations of wind-driven emission processes, for example, in the Multiple-scale Atmospheric Transport and Chemistry model (Andersson et al., 2015), in the System for Integrated Modelling of Atmospheric Composition (Sofiev et al., 2011), and in the model of the Co-operative Programme for Monitoring and Evaluation of the Long-range Transmission of Air Pollutants in Europe (Simpson et al., 2012). While multi-modal lognormal distributions can have a large number of free parameters, the power-law distribution only depends on N_1 and α, which makes it attractive for retrievals. N_1 depends mainly on wind speed, while α can be modeled as a function of salinity and sea-surface temperature (Sofiev et al., 2011). Over the oceans, α typically varies between 0 and 1, but for freshwater it can be as high as 3 (Sofiev et al., 2011). In place of α, the effective dry radius will be used to describe the optical size of an ensemble of particles, which is defined by

$$r_{\mathrm{eff}}^{\mathrm{dry}} = \frac{\int_0^\infty r^3 n(r)\mathrm{d}r}{\int_0^\infty r^2 n(r)\mathrm{d}r}, \quad (2)$$

where $n(r)$ describes the size-distribution of volume-equivalent dry radii r. This quantity describes that effective radius that the ensemble of particles would have if all water were removed. It provides a convenient size-measure to compare particles with different water content (i.e., different salt-mass fractions f_{m}). But it is emphasized that the hygroscopic growth of the particles is explicitly accounted for in the model. For each salt-mass fraction the

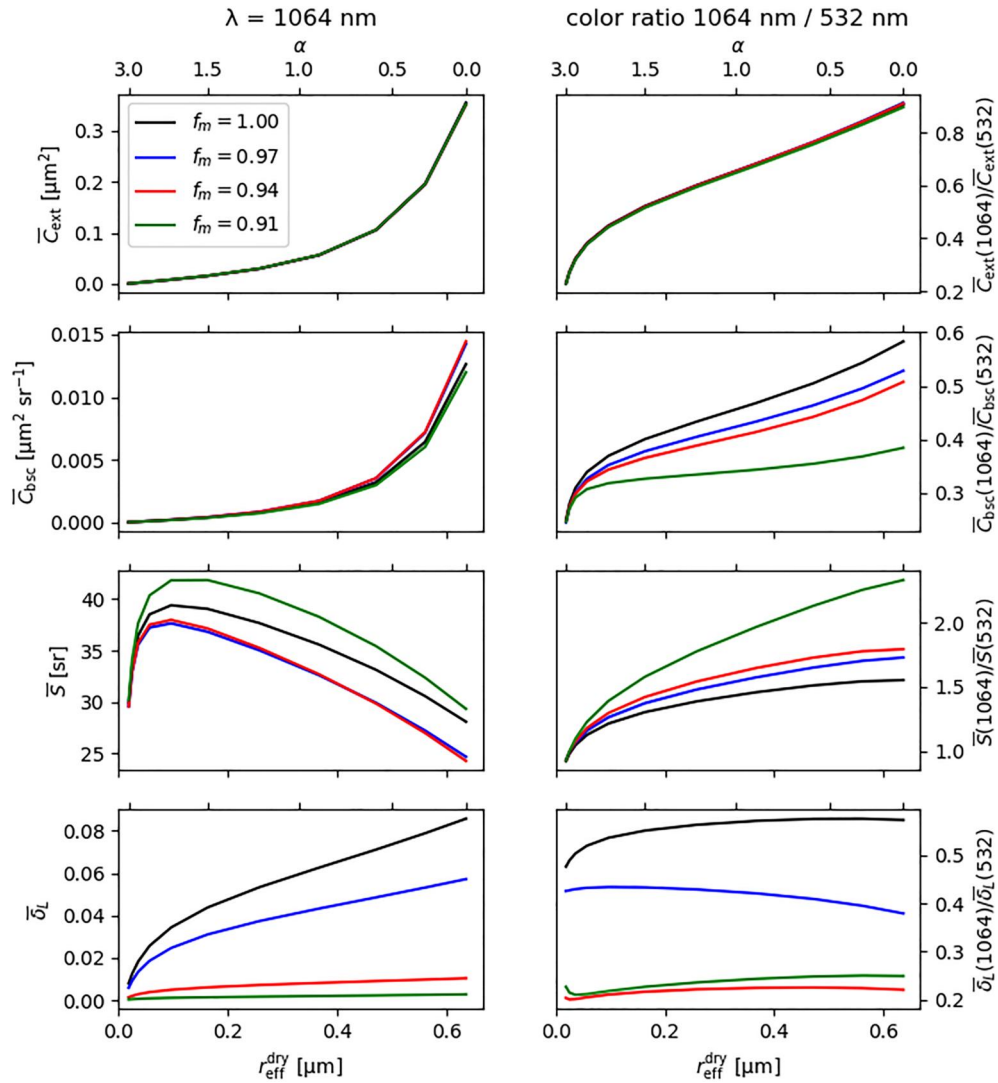

Figure 2. Left: size-averaged optical properties at 1,064 nm wavelength as a function of effective dry radius for different salt mass fractions f_m, first row: extinction cross section, 2nd row: backscattering cross section, third row: lidar ratio, fourth row: linear depolarization ratio. Right: corresponding color ratios of optical properties at 1,064 nm and 532 nm.

distribution of wet radii is computed from that of dry radii based on the method outlined in Section 2.1—see also Kahnert and Kanngießer (2023a).

3. Results

3.1. Optical Properties Relevant for Active Remote Sensing

Figure 2 shows size-averaged optical properties for different values of the salt mass fraction f_m. The left column displays results obtained for $\lambda_1 = 1{,}064$ nm, and the right column shows the corresponding color ratios with respect to λ_1 and $\lambda_2 = 532$ nm. Optical properties are shown as a function of the effective dry radius $r_{\rm eff}^{\rm dry}$. However, it is emphasized that wet particles ($f_m < 1$) have wet radii that are slightly larger than the dry radii due to the addition of water, which is accounted for in the model (see Section 2.1). We chose to use the dry radii as a common reference in this figure in order to show more clearly to what extent the addition of water (decreasing $f_m < 1$) impacts the optical cross sections.

The extinction cross section $\bar{C}_{\rm ext}$ (top right) is strongly dependent on $r_{\rm eff}^{\rm dry}$, yet quite insensitive to changes in f_m. This is because within the limited range of salt-mass fraction considered here, the wet radius is not dramatically

larger than the corresponding dry radius. (As an example, a particle with dry radius 1.5 μm and a salt-mass fraction of 0.91 would have a wet radius of 1.6 μm—see also Figure 11 by Kahnert and Kanngießer (2023a).) Further, the corresponding color ratio (top right) is also insensitive to a variation in f_m. In lidar remote sensing, one can use the extinction cross section $k = N\bar{C}_{ext}$ and its color ratio $k(\lambda_1)/k(\lambda_2) = \bar{C}_{ext}(\lambda_1)/\bar{C}_{ext}(\lambda_2)$ to retrieve the aerosol number density N and the effective radius of the particles (as the color ratio is only dependent on size, but not N). The results indicate that, within the range of salt-mass fractions considered here, this is a robust approach unaffected by varying values of f_m.

By contrast, the color ratio of the backscattering cross section (2nd row right) is monotonically decreasing with decreasing f_m. This indicates that independent observations of extinction and backscattering at two wavelengths should allow us to simultaneously retrieve N, r_{eff}^{dry}, and f_m.

The third row shows that the lidar ratio $\bar{S}(\lambda_1)$ is strongly dependent on both r_{eff}^{dry} and f_m; it varies between 25 and 43 sr. The color ratio of $\bar{S}$ ranges between about 1 and 2.5. In the processing of CALIPSO observations, backscattering and extinction coefficients are obtained from attenuated backscattering measurements by assuming fixed lidar ratios for each type of aerosol. For instance, Omar et al. (2009) list lidar ratios for clean marine aerosols of 20 and 45 sr at 532 and 1,064 nm, respectively, corresponding to $\bar{S}(\lambda_1)/\bar{S}(\lambda_2) = 2.25$. According to the results obtained here, $\bar{S}(\lambda_1) = 45$ sr would be representative of $r_{eff}^{dry} = 0.1$ μm and $f_m = 0.91$, while a color ratio of 2.25 would be characteristic of $r_{eff}^{dry} = 0.5$ μm and $f_m = 0.91$. In the latest version 4 of the CALIPSO automated aerosol classification and lidar ratio selection algorithm (Kim et al., 2018), a spectrally neutral lidar ratio of 23 ± 5 sr at 532 and 1,064 nm is being assumed. This is based on several recent studies (Haarig et al., 2017; Josset et al., 2012; Müller et al., 2007; Papagiannopoulos et al., 2016; Rogers et al., 2014; Sayer et al., 2012). According to the modeling results in Figure 2 (third row), a lidar ratio of 23 at 1,064 nm would be representative of relatively dry, large particles with $r_{eff}^{dry} \geq 0.6$ μm, while a color ratio of 1 would suggest particles with $r_{eff}^{dry} \leq 0.05$ μm. This shows that there are some remaining challenges in reconciling light-scattering models with lidar-ratio assumptions made in the retrieval of backscattering and extinction coefficients. The model considered here suggests that both $\bar{S}$ and its color ratio depend on both r_{eff}^{dry} and f_m.

Similarly, the linear depolarization ratio δ_L (bottom left) depends strongly on r_{eff}^{dry} and f_m. As more water is being adsorbed (and f_m decreases), the particles become more spherical, resulting in a quenching of δ_L. Thus, depolarization provides useful information on the water content of marine aerosol, but only to the point at which the particles become spherical. The relatively low color ratios (bottom right) show that depolarization is strongest in the visible part of the spectrum. Also, for $f_m \leq 0.94$ the color ratio of δ_L is probably not helpful, as it is based on division of two very small values. Thus, to constrain the water content of marine aerosols in the transition regime from nonspherical crystals to spherical droplets it is likely to be sufficient to measure δ_L at a single wavelength, that is, at $\lambda_2 = 532$ nm.

3.2. Optical Properties Relevant for Passive Remote Sensing

The phase function (not shown) is relatively flat and featureless at side-scattering angles, which is typical for size-shape distributions of aerosols. The diffraction peak in the forward direction becomes more intense and more narrow with increasing size parameter $x = 2\pi r_{eff}^{dry}/\lambda$.

The phase-matrix element $-F_{12}/F_{11}$ has some distinct properties. This quantity describes the degree of linear polarization generated in single-scattering events of unpolarized sunlight. Figure 3 presents $-F_{12}/F_{11}$ as a function of the scattering angle and r_{eff}^{dry} for different values of f_m (across rows), as well as for two wavelengths (across columns), as indicated in the panels. A most prominent feature is the negative polarization peaking at scattering angles around 161–163°. A similar feature has been observed by Bi, Lin, Wang, et al. (2018), using a geometrically simpler model of core-mantle superellipsoids. Inspection of Figures 12 and 13 in that paper indicates that the negative polarization branch is more pronounced for spherical particles, and it is enhanced by inhomogeneity. A comparison of homogeneous spheres, two super-spheroids, and three inhomogeneous spheres with both spherical and nonspherical cores presented by M. Li et al. (2022) arrived at conclusions consistent with those by Bi, Lin, Wang, et al. (2018). Similarly, it can be seen here in Figure 3 that the negative polarization intensifies with increasing water content (decreasing f_m), that is, as the particles become more spherical. Further,

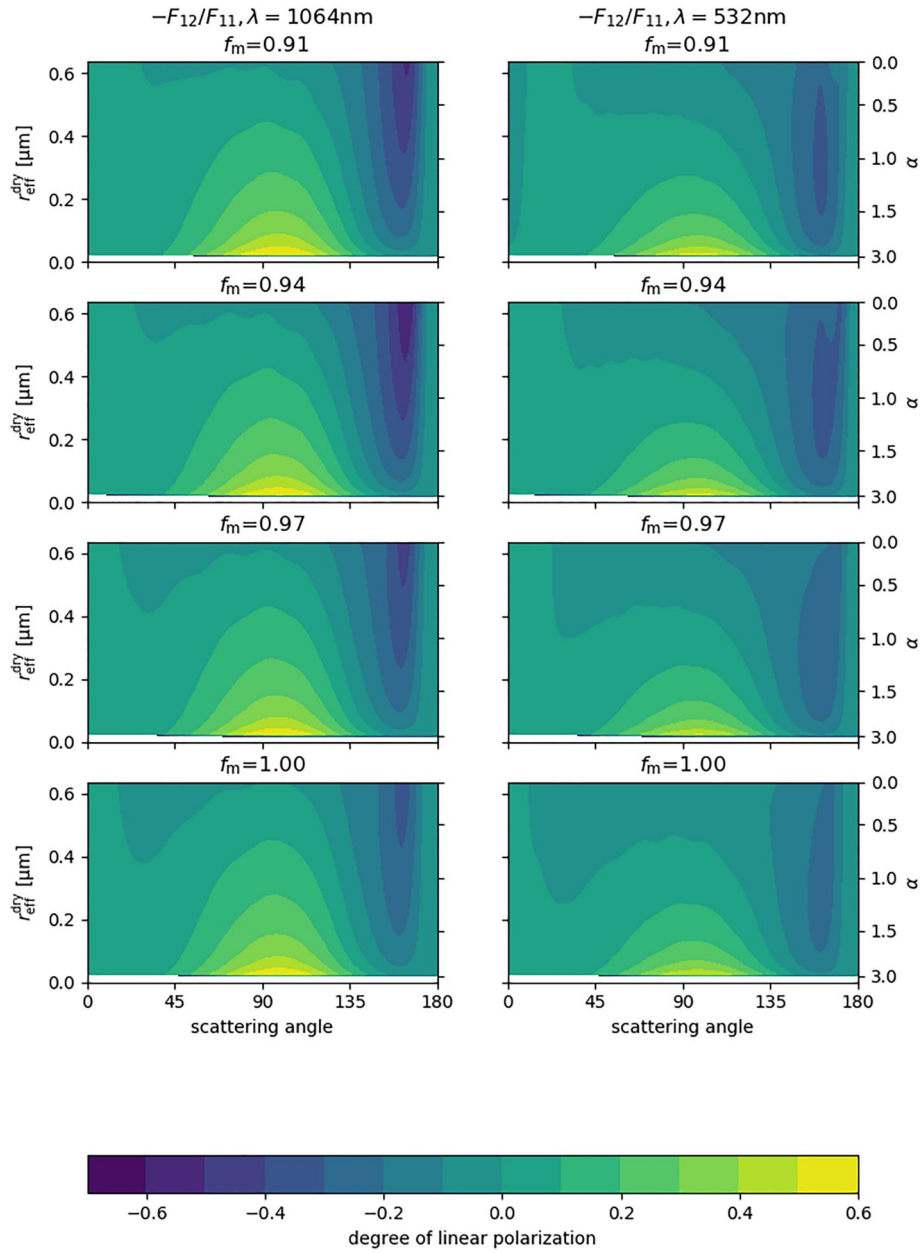

Figure 3. Degree of linear polarzation $-F_{12}/F_{11}$ as a function of scattering angle and effective dry radius for different f_m (across rows), and for $\lambda_1 = 1{,}064$ nm (left column) and $\lambda_2 = 532$ nm (right column).

the negative polarization peak is more pronounced in the IR (left) than in the visible part of the spectrum (right), and it intensifies with growing r_{eff}^{dry}. These findings suggest that observation of linearly polarized scattered sunlight in the near infrared (NIR) at scattering angles around 162° could provide a passive polarimetric method for inferring the water content of marine aerosols.

M. Li et al. (2023) employed coated super-spheroids, including coated spheres, to investigate the range of size parameters, shell-core ratios, and refractive indices for which the negative polarization at near-backscattering directions is most pronounced. They concluded that the negative polarization is most pronounced for weakly absorbing particles with size parameters ≤14.5 and shell-core ratios around 1.4–1.9, where the latter is defined as the ratio of the size parameters of the shell and the core, respectively.

4. Conclusions

A study of the optical properties of morphologically realistic brine-coated sea salt particles has been presented, which led to the following findings.

1. The ensemble-averaged extinction cross section $\bar{C}_{\text{ext}}$ strongly depends on the effective radius of the particles. The same is true for the color ratio $\bar{C}_{\text{ext}}(\lambda_1)/\bar{C}_{\text{ext}}(\lambda_2)$, where $\lambda_1 = 1{,}064$ nm and $\lambda_2 = 532$ nm. Neither the extinction cross section nor the corresponding color ratio changes much with the salt mass fraction f_{m}. The extinction coefficient $k = N\bar{C}_{\text{ext}}$ depends on both the number density and the extinction cross section. Thus, the color ratio of k, which does not depend on N, can be used to retrieve particle size. Simultaneous measurements of k at two wavelengths should provide a robust method for simultaneous retrieval of particle size and number density, unperturbed by variations in water content. Although measurements of the extinction coefficient at NIR wavelengths is challenging, encouraging progress with Raman lidar techniques has been reported (Haarig et al., 2016).
2. The lidar ratio varies considerably with particle size and salt mass fraction (between 25 and 43 sr at $\lambda = 1{,}064$ nm); its color ratio varies between 1 and 2.5. High-level lidar products (such as level 2 and level 3 CALIPSO products) assume fixed values of the lidar ratio in retrieving extinction and backscattering coefficients from attenuated backscattering signals. The results of the present study suggest that such retrievals may have systematic errors owning to the pronounced dependence of the lidar ratio on particle size and water content. A reliable retrieval of particle size, composition, and number density would need to invert the lidar equation by taking the size- and wavelength-dependence of the lidar ratio into account. This is a challenging inverse problem, since the lidar ratio required for solving the lidar equation is size dependent, but the size of the particles is one of the quantities one wants to retrieve from the solution of the lidar equation.
3. Both the color ratio $\bar{C}_{\text{bsc}}(\lambda_1)/\bar{C}_{\text{bsc}}(\lambda_2)$ of the backscattering cross section (or the backscattering coefficient) and the depolarization ratio δ_L generally increase with growing salt mass fraction f_{m} and with particle size. δ_L is larger in the visible than in the NIR part of the spectrum. Hence, both the backscattering color ratio and δ_L at 532 nm provide quantitative information on the water content of marine aerosols. Additional observation of δ_L at 1,064 nm is not expected to provide much extra information on the water content.
4. The degree of linear polarization of sunlight scattered at specific angles can be strongly modulated by the water content of the aerosols. This effect is most pronounced in the NIR part of the spectrum at scattering angles around 162°, which could open up new possibilities in passive polarimetric remote sensing to estimate the water content of marine aerosols.
5. At $\lambda_2 = 532$ nm, dry sea salt particles can have a depolarization ratio δ_L up to 0.15, which is higher than that of uncoated soot aerosols (e.g., Burton et al., 2015; Kanngießer & Kahnert, 2018; Kahnert & Kanngießer, 2020), and considerably lower than that of mineral dust aerosols (e.g., Burton et al., 2015; Kahnert et al., 2020). This can help to disentangle mixed aerosol populations, as is done in CALIPSO aerosol classifications (Omar et al., 2009), but also in quantitative retrievals based on field measurements (e.g., David et al. (2013)).

The computations performed in this study were limited to dry radii up to 1.5 μm and wet radii up to roughly 1.6 μm. Marine aerosols in nature can contain larger particles, typically up to or even exceeding 5 μm radius, even though larger particles often have low number densities. This limits the model to serving, mostly, as a reference model in theoretical studies. In quantitative applications, such as retrieval methods in remote sensing or chemical data assimilation, one will need to rely on simpler and faster models that are capable of covering the full range of relevant particle sizes, at least up to 5 μm.

Data Availability Statement

Version 1.3b4 of the discrete-dipole approximation code ADDA (Yurkin & Hoekstra, 2011), which was used to compute the optical properties, is publicly available via GPLv3 license at https://github.com/adda-team/adda. The computed optical properties have been published (Kahnert & Kanngießer, 2023b) under the Creative Commons Attribution 4.0 International licence and can be downloaded at Zenodo, https://zenodo.org/records/10203860.

Acknowledgments
The authors are indebted to M. Yurkin and A. Hoekstra for making the ADDA code publicly available. Funding by the Swedish National Space Agency is acknowledged (contracts 126/19, 2022-00148).

References

Andersson, C., Bergström, R., Bennet, C., Robertson, L., Thomas, M., Korhonen, H., et al. (2015). MATCH-SALSA—Multi-scale Atmospheric Transport and CHemistry model coupled to the SALSA aerosol microphysics model—Part 1: Model description and evaluation. *Geoscientific Model Development*, *8*(2), 171–189. https://doi.org/10.5194/gmd-8-171-2015

Bi, L., Lin, W., Liu, D., & Zhang, K. (2018). Assessing the depolarization capabilities of nonspherical particles in super-ellipsoidal shape space. *Optics Express*, *26*(2), 1726–1742. https://doi.org/10.1364/oe.26.001726

Bi, L., Lin, W., Wang, Z., Tang, X., Zhang, X., & Yi, B. (2018). Optical modeling of sea salt aerosols: The effects of nonsphericity and inhomogeneity. *Journal of Geophysical Research*, *123*(1), 543–558. https://doi.org/10.1002/2017jd027869

Burton, S. P., Hair, J. W., Kahnert, M., Ferrare, R. A., Hostetler, C. A., Cook, A. L., et al. (2015). Observations of the spectral dependence of particle depolarization ratio of aerosols using NASA Langley airborne High Spectral Resolution Lidar. *Atmospheric Chemistry and Physics*, *15*(23), 13453–13473. https://doi.org/10.5194/acp-15-13453-2015

Dai, G., Wu, S., Long, W., Liu, J., Xie, Y., Sun, K., et al. (2023). Aerosols and Clouds data processing and optical properties retrieval algorithms for the spaceborne ACDL/DQ-1. *EGUsphere, 2023*, 1–20. https://doi.org/10.5194/egusphere-2023-2182

David, G., Thomas, B., Nousiainen, T., Miffre, A., & Rairoux, P. (2013). Retrieving simulated volcanic, desert dust and sea-salt particle properties from two/three-component particle mixtures using UV-VIS polarization lidar and T matrix. *Atmospheric Chemistry and Physics*, *13*(14), 6757–6776. https://doi.org/10.5194/acp-13-6757-2013

Eldridge, J., & Palik, E. D. (1997). Sodium chloride (NaCl). In E. D. Palik (Ed.), *Handbook of optical constants of solids* (pp. 775–793). Academic Press. https://doi.org/10.1016/B978-012544415-6.50041-8

Ferrare, R., Hair, J., Hostetler, C., Shingler, T., Burton, S. P., Fenn, M., et al. (2023). Airborne HSRL-2 measurements of elevated aerosol depolarization associated with non-spherical sea salt. *Frontiers in Remote Sensing*, *4*, 1143944. https://doi.org/10.3389/frsen.2023.1143944

Fitzgerald, J. W. (1975). Approximation formulas for the equilibrium size of an aerosol particle as a function of its dry size and composition and the ambient relative humidity. *Journal of Applied Meteorology*, *14*(6), 1044–1048. https://doi.org/10.1175/1520-0450(1975)014<1044:afftes>2.0.co;2

Gerber, H. E. (1985). *Relative-humidity parameterization of the Navy Aerosol Model (NAM) (Tech. Rep. No. 8956)*. Naval Research Laboratory.

Gwaze, P., Helas, G., Annegarn, H. J., Huth, J., & Piketh, S. J. (2007). Physical, chemical and optical properties of aerosol particles collected over Cape Town during winter haze episodes. *South African Journal of Science*, *103*, 35–43.

Haarig, M., Ansmann, A., Gasteiger, J., Kandler, K., Althausen, D., Baars, H., et al. (2017). Dry versus wet marine particle optical properties: RH dependence of depolarization ratio, backscatter, and extinction from multiwavelength lidar measurements during SALTRACE. *Atmospheric Chemistry and Physics*, *17*(23), 14199–14217. https://doi.org/10.5194/acp-17-14199-2017

Haarig, M., Engelmann, R., Ansmann, A., Veselovskii, I., Whiteman, D. N., & Althausen, D. (2016). 1064 nm rotational Raman lidar for particle extinction and lidar-ratio profiling: Cirrus case study. *Atmospheric Measurement Techniques*, *9*(9), 4269–4278. https://doi.org/10.5194/amt-9-4269-2016

Ishimoto, H., Kudo, R., & Adachi, K. (2019). A shape model of internally mixed soot particles derived from artificial surface tension. *Atmospheric Measurement Techniques*, *12*(1), 107–118. https://doi.org/10.5194/amt-12-107-2019

Josset, D., Pelon, J., Hu, Y., Rogers, R., Liu, Z., Omar, A., et al. (2012). Global scale lidar ratio retrieval over the ocean. In *26th international laser radar conference (ILRC 26)*. Retrieved from https://hal.science/hal-00722435

Kahnert, M., & Kanngießer, F. (2020). Modelling optical properties of atmospheric black carbon aerosols. *Journal of Quantitative Spectroscopy & Radiative Transfer*, *244*, 106849. https://doi.org/10.1016/j.jqsrt.2020.106849

Kahnert, M., & Kanngießer, F. (2023a). Optical properties of marine aerosol: Modelling the transition from dry, irregularly shaped crystals to brine-coated, dissolving salt particles. *Journal of Quantitative Spectroscopy & Radiative Transfer*, *295*, 108408. https://doi.org/10.1016/j.jqsrt.2022.108408

Kahnert, M., & Kanngießer, F. (2023b). Optical properties of marine aerosols with varying water content at wavelengths 532 and 1064 nm, modelled with a morphologically realistic aerosol model (1.0) [Dataset]. Zenodo. https://doi.org/10.5281/zenodo.10203860

Kahnert, M., Kanngießer, F., Järvinen, E., & Schnaiter, M. (2020). Aerosol-optics model for the backscatter depolarisation ratio of mineral dust particles. *Journal of Quantitative Spectroscopy & Radiative Transfer*, *254*, 107177. https://doi.org/10.1016/j.jqsrt.2020.107177

Kanngießer, F., & Kahnert, M. (2018). Calculation of optical properties of light-absorbing carbon with weakly absorbing coating: A model with tunable transition from film-coating to spherical-shell coating. *Journal of Quantitative Spectroscopy & Radiative Transfer*, *2016*, 17–36.

Kanngießer, F., & Kahnert, M. (2021a). Modeling optical properties of non-cubical sea-salt particles. *Journal of Geophysical Research: Atmospheres*, *126*(4), e2020JD033674. https://doi.org/10.1029/2020jd033674

Kanngießer, F., & Kahnert, M. (2021b). Optical properties of water-coated sea salt model particles. *Optics Express*, *29*(22), 34926–34950. https://doi.org/10.1364/oe.437680

Kim, M.-H., Omar, A. H., Tackett, J. L., Vaughan, M. A., Winker, D. M., trepte, C. R., et al. (2018). The CALIPSO version 4 automated aerosol classification and lidar ratio selection algorithm. *Atmospheric Measurement Techniques*, *11*, 6107–6135. https://doi.org/10.5194/amt-11-6107-2018

King, S. M., Butcher, A. C., Rosenoern, T., Coz, E., Lieke, K. I., de Leeuw, G., et al. (2012). Investigating primary marine aerosol properties: CCN activity of sea salt and mixed inorganic-organic particles. *Environmental Science & Technology*, *46*(19), 10405–10412. https://doi.org/10.1021/es300574u

Li, M., Bi, L., & Lin, W. (2023). Distinct linear polarization of core-shell particles at near-backscattering directions. *Optics Express*, *31*(26), 44648–44671. https://doi.org/10.1364/oe.509240

Li, M., Bi, L., Lin, W., Weng, F., He, S., & Zhang, X. (2022). The inhomogeneity effect of sea salt aerosols on the TOA polarized radiance at the scattering angles ranging from 170° to 175°. *IEEE Transactions on Geoscience and Remote Sensing*, *60*, 1–12. https://doi.org/10.1109/tgrs.2021.3099026

Li, X., Liu, L., Zhao, J., & Tan, J. (2015). Optical properties of sodium chloride solution within the spectral range from 300 to 2500 nm at room temperature. *Applied Spectroscopy*, *69*(5), 635–640. https://doi.org/10.1366/14-07769r

Li, X., Liu, L., Zhao, J., & Tan, J. (2018). Corrigendum: Optical properties of sodium chloride solution within the spectral range from 300 to 2500 nm at room temperature. *Applied Spectroscopy*, *72*(8), 1277.

Liu, Q., Huang, Z., Liu, J., Chen, W., Dong, Q., Wu, S., et al. (2023). Validation of initial observation from the first space-borne high spectral resolution lidar with ground-based lidar network. *Atmospheric Measurement Techniques Discussions*, *2023*, 1–28. https://doi.org/10.5194/amt-2023-235

Mårtensson, E. M., Nilsson, E. D., de Leeuw, G., Cohen, L. H., & Hansson, H.-C. (2003). Laboratory simulations and parameterization of the primary marine aerosol production. *Journal of Geophysical Research*, *108*(D9), 4297. https://doi.org/10.1029/2002jd002263

McInnes, L. M., Covert, D. S., Quinn, P. K., & Germani, M. S. (1994). Measurements of chloride depletion and sulfur enrichment in individual sea-salt particles collected from the remote marine boundary layer. *Journal of Geophysical Research*, *99*(D4), 8257–8268. https://doi.org/10.1029/93JD03453

Monahan, E. C., Spiel, D. E., & Davidson, K. L. (1986). A model of marine aerosol generation via whitecaps and wave disruption. In E. C. Monahan & G. M. Niocaill (Eds.), *Oceanic whitecaps and their role in air-sea exchange* (pp. 167–174). Springer Science & Business Media.

Müller, D., Ansmann, A., Mattis, I., Tesche, M., Wandinger, U., Althausen, D., & Pisani, G. (2007). Aerosol-type-dependent lidar ratios observed with Raman lidar. *Journal of Geophysical Research*, *112*(D16), D16202. https://doi.org/10.1029/2006jd008292

Omar, A. H., Winker, D. M., Vaughan, M. A., Hu, Y., Trepte, C. R., Ferrare, R. A., et al. (2009). The CALIPSO automated aerosol classification and lidar ratio selection algorithm. *Journal of Atmospheric and Oceanic Technology*, *26*(10), 1994–2014. https://doi.org/10.1175/2009jtecha1231.1

Papagiannopoulos, N., Mona, L., Alados-Arboledas, L., Amiridis, V., Baars, H., Binietoglou, I., et al. (2016). CALIPSO climatological products: Evaluation and suggestions from EARLINET. *Atmospheric Chemistry and Physics*, *16*(4), 2341–2357. https://doi.org/10.5194/acp-16-2341-2016

Patterson, J. P., Collins, D. B., Michaud, J. M., Axson, J. L., Sultana, C. M., Moser, T., et al. (2016). Sea spray aerosol structure and composition using cryogenic transmission electron microscopy. *ACS Central Science*, *2*(1), 40–47. https://doi.org/10.1021/acscentsci.5b00344

Peart, A., & Evans, J. R. G. (2011). Study of sea salt particles launched by bubble burst. *Bubble Science, Engineering and Technology*, *3*(2), 64–72. https://doi.org/10.1179/1758897911Y.0000000004

Rogers, R. R., Vaughan, M. A., Hostetler, C. A., Burton, S. P., Ferrare, R. A., Young, S. A., et al. (2014). Looking through the haze: Evaluating the CALIPSO level 2 aerosol optical depth using airborne high spectral resolution lidar data. *Atmospheric Measurement Techniques*, *7*(12), 4317–4340. https://doi.org/10.5194/amt-7-4317-2014

Sayer, A. M., Smirnov, A., Hsu, N. C., & Holben, B. N. (2012). A pure marine aerosol model, for use in remote sensing applications. *Journal of Geophysical Research*, *117*(D5), D05213. https://doi.org/10.1029/2011jd016689

Simpson, D., Benedictow, A., Berge, H., Bergström, R., Emberson, L. D., Fagerli, H., et al. (2012). The EMEP MSC-W chemical transport model —Technical description. *Atmospheric Chemistry and Physics*, *12*(16), 7825–7865. https://doi.org/10.5194/acp-12-7825-2012

Soares, J., Sofiev, M., Geels, C., Christensen, J. H., Andersson, C., Tsyro, S., & Langner, J. (2016). Impact of climate change on the production and transport of sea salt aerosol on European seas. *Atmospheric Chemistry and Physics*, *16*(20), 13081–13104. https://doi.org/10.5194/acp-16-13081-2016

Sofiev, M., Soares, J., Prank, M., de Leeuw, G., & Kukkonen, J. (2011). A regional-to-global model of emission and transport of sea salt particles in the atmosphere. *Journal of Geophysical Research*, *116*(D21), D21302. https://doi.org/10.1029/2010jd014713

Thomas, M. A., Devasthale, A., & Kahnert, M. (2022). Marine aerosol properties over the Southern Ocean in relation to the wintertime meteorological conditions. *Atmospheric Chemistry and Physics*, *22*(1), 119–137. https://doi.org/10.5194/acp-22-119-2022

Wang, H., Dai, T., Goto, D., Bao, Q., He, B., Liu, Y., et al. (2020). Simulating and evaluating global aerosol distributions with the online aerosol-coupled CAS-FGOALS model. *Journal of Geophysical Research*, *125*(24), e2019JD032097. https://doi.org/10.1029/2019JD032097

Wang, Z., Bi, L., Yi, B., & Zhang, X. (2019). How the inhomogeneity of wet sea salt aerosols affects direct radiative forcing. *Geophysical Research Letters*, *46*(3), 1805–1813. https://doi.org/10.1029/2018gl081193

Wise, M. E., Biskos, G., Martin, S. T., Russell, L. M., & Buseck, P. R. (2005). Phase transitions of single salt particles studied using a transmission electron microscope with an environmental cell. *Aerosol Science & Technology*, *39*(9), 849–856. https://doi.org/10.1080/02786820500295263

Yurkin, M. A., & Hoekstra, A. G. (2011). The discrete-dipole-approximation code ADDA: Capabilities and known limitations. *Journal of Quantitative Spectroscopy & Radiative Transfer*, *112*(13), 2234–2247. https://doi.org/10.1016/j.jqsrt.2011.01.031

Zeng, J., Zhang, G., Long, S., Liu, K., Cao, L., Bao, L., & Li, Y. (2013). Sea salt deliquescence and crystallization in atmosphere: An in situ investigation using X-ray phase contrast imaging. *Surface and Interface Analysis*, *45*(5), 930–936. https://doi.org/10.1002/sia.5184

Zhu, L., Shu, S., Wang, Z., & Bi, L. (2022). More or less: How do inhomogeneous sea-salt aerosols affect the precipitation of landfalling tropical cyclones? *Geophysical Research Letters*, *49*(3), e2021GL097023. https://doi.org/10.1029/2021gl097023